DOI: 10.1002/ejic.200500743

Optical Properties of the Perovskite Solid Solution $LaTiO_2N$–$ATiO_3$ (A = Sr, Ba)

François Cheviré,[a] Franck Tessier,*[a] and Roger Marchand[a]

Keywords: Oxynitrides / Perovskites / Solid solution / Optical properties

Starting from the colored oxynitride $LaTiO_2N$, new perovskite-type solid solutions have been evidenced in the systems $La_{1-x}A_xTiO_{2+x}N_{1-x}$ (A = Sr, Ba) by ammonolysis at 950 °C of the corresponding oxide precursors prepared by the molten salt route. The color of the resulting powders varies progressively from the brown of $LaTiO_2N$ to the white of the oxide with a decrease in both the nitrogen and lanthanum contents. The optical absorption was characterized by diffuse reflectance. The nonlinear variation of the optical bandgap may result from the competition between the variation of the inductive effect between lanthanum and strontium, structural changes, and the difference in electronegativity between nitrogen and oxygen. For the compounds with a low nitrogen content the observed green shade is attributed to the presence of a nitrogen-rich secondary phase: TiO_xN_y in which titanium presents a mixed-valence state. Taking advantage of a chimie douce process, the amorphous citrate route, the highest oxidation state of titanium was stabilized until $x = 0.9$ in the $La_{0.1}Sr_{0.9}Ti(O,N)_3$ phase giving the powder a bright yellow color (Eg = 2.49 eV).
(© Wiley-VCH Verlag GmbH & Co. KGaA, 69451 Weinheim, Germany, 2006)

Introduction

The progressive insertion of nitrogen, a less electronegative element compared with oxygen, within an oxide network involves an increase in the covalency of the bonding. A lower optical gap value, Eg, and consequently a modification of the absorption properties of the compound results from this substitution. Whereas many oxides are white, the corresponding oxynitrides are often colored. For example, considering the following cross-substitution: $M^{n+} + O^{2-} = M^{(n+1)+} + N^{3-}$, ZrO_2 (baddeleyite) and $BaTiO_3$ (perovskite) give rise to the isostructural colored oxynitrides TaON (yellow, Eg = 2.5 eV) and $BaTaO_2N$ (red brown, Eg = 2.0 eV), respectively. Over the last few years, nitride-type materials have largely been studied for their optical potential as nontoxic colored pigments (see below), as novel inorganic UV absorbers,[1] or as visible light-driven photocatalysts.[2–5]

The first colored oxynitride perovskites were obtained by substituting titanium in $BaTiO_3$ by a +5 oxidation-state element, such as tantalum or niobium. Numerous novel oxynitride phases were and are still obtained by applying this substitution principle at both the 12- and 6-fold-coordinated cationic sites. This is a key principle at the origin of a rich chemistry. $ATaO_2N$ (A = Ca, Sr, Ba) and $ANbO_2N$ (A = Sr, Ba) manifest dielectric properties.[6,7] $BaTaO_2N$ and $BaNbO_2N$ crystallize in a cubic unit cell and $SrTaO_2N$ in a tetragonal one.[8–10] The substitution of barium by a lanthanide element results in the oxynitrides $RTiO_2N$ (R = La, Nd),[11] where the +4 oxidation state of titanium is stabilized by the inductive effect of the rare earth element on the Ti-(O,N) bond.[12,13] This well-known effect is based on the capacity of an electropositive element (alkaline earth or rare earth) to share some electrons with the closest transition metal–nitrogen (oxygen) bond to enhance its covalent character, and thus to stabilize it. $NdTiO_2N$ is an orthorhombic $GdFeO_3$-type perovskite, while $LaTiO_2N$ crystallizes in a unit cell with triclinic symmetry.[14] The simultaneous substitution of both barium and titanium enables access to the white phase $LaZrO_2N$, which also presents a deformed $GdFeO_3$-type perovskite structure,[14] or to the oxynitride family $RTaON_2$ (R = La → Dy) and $LaNbON_2$.[11]

On the basis of one of the specific features of nitrogen, i.e. $\chi_N < \chi_O$, we were very interested in working with oxynitride solid-solution domains as a suitable means to tune the optical properties by the progressive modification of the composition. Jansen et al. have shown the possibility of adjusting the color of oxynitride pigments in the perovskite-type system $Ca_{1-x}La_xTaO_{2-x}N_{1+x}$.[15,16] The hue varies from yellow ($CaTaO_2N$) to brown ($LaTaON_2$) through orange and red intermediate colors as a result of the nitrogen content. Grins et al. obtained similar results in the system $AZr_{1-x}Ta_xO_{3-x}N_x$ with powders evolving from the white of $AZrO_3$ to the yellow, red, or brown of $ATaO_2N$, where A corresponds to Ca, Sr, and Ba, respectively.[17] Recently, Diot has evidenced solid-solution domains in the perovskite systems $A(A,Ta)(O,N,\square)_3$ (A = Ca, Sr, Ba) and

[a] UMR CNRS 6512 "Verres et Céramiques", Institut de Chimie de Rennes, Université de Rennes 1,
35042 Rennes cedex, France
Fax: +33-2-23235683
Franck.Tessier@univ-rennes1.fr

 © 2006 Wiley-VCH Verlag GmbH & Co. KGaA, Weinheim

$Sr(Sr,Nb)(O,N,\square)_3$ giving rise to a range of colored pigments from pale yellow to orange brown.[18] Her research has also shown the interest in using defect fluorite rare earth tungstates $R_6WO_{12}\square_2$ and $R_{14}W_4O_{33}\square_3$ (R = rare earth) to isolate oxynitride powders $R_6W(O,N,\square)_{14}$ and $R_{14}W_4(O,N,\square)_{36}$, the color of which changes progressively from the white of the oxides to bright yellow with increasing nitrogen substitution. While with large rare earth elements the ammonolysis reaction of $RTaO_4$ tantalates provides either perovskite phases $RTaON_2$[11] or pyrochlore phases $R_2Ta_2O_5N_2$,[19] Maillard et al. identified defect fluorite solid solutions $RTa(O,N,\square)_4$ with small rare earths ($r_{R3+} \leq r_{Gd3+}$).[20] Colored oxynitride solid-solution domains have also been obtained in other structure types; for example, orange $Ta_{3-x}Zr_xN_{5-x}O_x$ ($0 \leq x \leq 0.60$) isostructural with Ta_3N_5 and pale yellow $Ta_{1-x}Zr_xN_{1-x}O_{1+x}$ ($0 \leq x \leq 0.28$) isostructural with TaON.[21]

This study was motivated, in part, by the preparation of light-colored oxynitride powders, for which an absorption edge located at exactly 400 nm will allow the absorption of all UV radiations. Our objective was to evidence a solid-solution domain $La_{1-x}A_xTiO_{2+x}N_{1-x}$ between the colored oxynitride $LaTiO_2N$ (brown, gap = 2.0 eV[22]) and the titanate $ATiO_3$ (A = Sr, Ba; gap > 3.1 eV) absorbing in the UV range.[1] $LaTiO_2N$ crystallizes in a distorted perovskite-type structure (Figure 1), as determined by neutron diffraction refinement, with a triclinic unit cell ($I\bar{1}$, a = 5.6097 Å, b = 7.8719 Å, c = 5.5772 Å, α = 90.199°, β = 90.154°, γ = 89.988°).[14] The structure reveals two distinct $Ti(O,N)_6$ octahedra and no nitrogen/oxygen ordering in the anionic network.

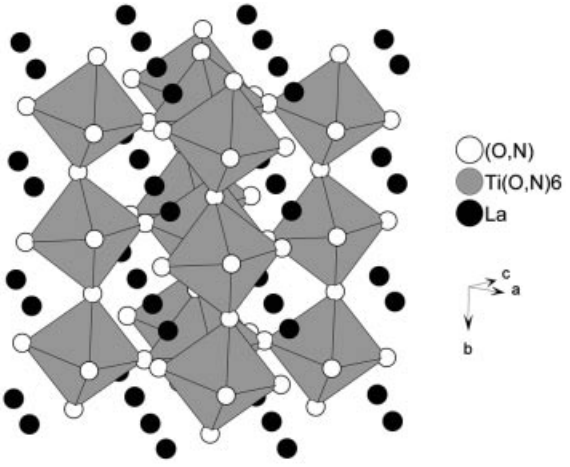

Figure 1. Crystal structure of the oxynitride perovskite $LaTiO_2N$.

Results and Discussion

Firstly, we have considered the preparation of oxide precursors by molten salt synthesis. When x = 0, $La_2Ti_2O_7$ (layered-perovskite structure) is clearly identified by X-ray diffraction. In the case of substituted compositions $La_{1-x}A_xTiO_y$, oxide precursors correspond generally to a mixture of ternary phases $La_aA_bTi_cO_d$ with variable composition. However, for x values close to 1, single-phase powders present a perovskite structure close to that of the corresponding $ATiO_3$ titanate. Interestingly, the reaction of these precursors under ammonia leads systematically to the formation of single-phase perovskite-type oxynitrides, even in the case of a mixture of multinary oxides ($x < 1$). Figure 2 clearly illustrates this observation with the example of the composition x = 0.5.

Table 1 details the experimental parameters of the ammonolysis experiments that were performed. All the compositions have a perovskite-structure type for which the position of the diffraction peaks continuously shifts from $LaTiO_2N$ to (Ba/Sr)TiO_3, as observed, for example, in the case of strontium (Figure 3). Although the structure of $LaTiO_2N$ was refined in a triclinic unit cell using neutron diffraction, the diffraction lines of the corresponding X-ray diffraction pattern can be indexed in a cubic perovskite unit cell [a = 3.939(2) Å]. The asymmetry of some peaks, previously reported,[11] indicates that the real unit cell is not cubic. However, the distortion is quite weak relative to that observed for $NdTiO_2N$ and is not strong enough to determine the unit cell unambiguously by this technique. Here, it was not our purpose to refine all compositions of the solid solution by neutron diffraction. Using the cubic unit cell is an easy way to verify the linear evolution of the cell parameter and to prove the formation of the solid solution. Corresponding cubic unit-cell parameters have been plotted vs. x in Figure 4. The trend follows a linear relation, in both cases, in agreement with Vegard's law. The opposite variation of the parameters, towards higher and lower values for Ba- and Sr-substitution, respectively, is explained if we compare the size of the cations in the 12-fold coordination (from Shannon:[23] La, 1.36 Å; Ba, 1.61 Å; Sr, 1.44 Å). There is a larger difference between La and Ba than there is for La and Sr, which should be balanced by the substitution of nitrogen by oxygen with increasing x values. The resulting effect of such a competition within the lattices leads to the observed trend.

The brown color of the Ba-containing oxynitrides slightly lightens when increasing the alkaline earth metal amount from x = 0.3 to 0.5. But the composition with x = 0.75 presents a dark green shade that we attribute to a partial reduction of titanium. A decrease in the reaction temperature to 900 °C does not modify the green aspect of the color. In the case of Sr-containing oxynitrides, we observe a different color range strongly related to the substitution of a smaller cation (Table 1). A study performed by Eng et al.[24] in the perovskite system $ATiO_3$ (A = Sr, Ca) attributes the formation of a narrow conduction band leading to a higher value of the bandgap (+0.2 eV) mainly to the distortion of the linear M–O–M bonds from Sr (180°) to Ca (156°). This effect becomes more detectable with Ta than with Ti compounds because of the formation of larger conduction bands. This study just focuses on the effect of the tilting of the octahedra and does not take into account

 © 2006 Wiley-VCH Verlag GmbH & Co. KGaA, Weinheim

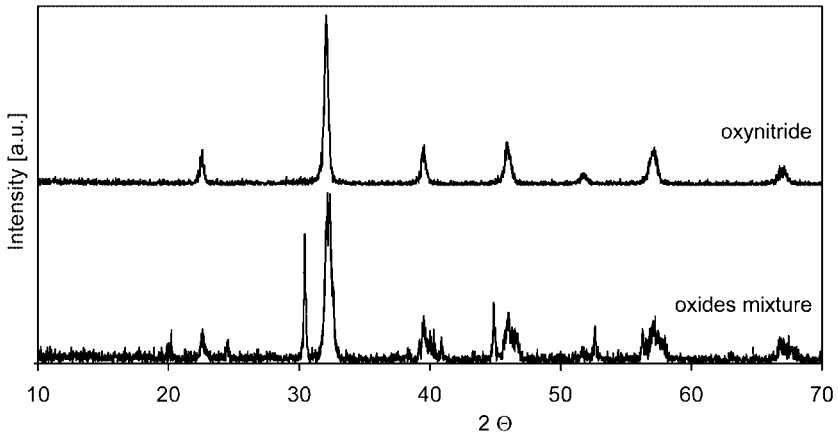

Figure 2. XRD powder pattern of the $La_{0.5}Ba_{0.5}TiO_{2.48}N_{0.52}$ oxynitride after ammonolysis of the corresponding oxide precursor.

Table 1. Experimental parameters for $La_{1-x}A_xTi(O,N)_3$ (A = Sr, Ba) oxynitrides.

Cationic composition	Nitridation parameters	Cubic unit-cell parameter[a] [Å]	Powder color
LaTi	950 °C/NH_3/15 h	3.939(2)	brown
$La_{0.90}Ba_{0.10}Ti$	950 °C/NH_3/15 h	3.945(2)	brown
$La_{0.70}Ba_{0.30}Ti$	950 °C/NH_3/15 h	3.970(3)	brown
$La_{0.50}Ba_{0.50}Ti$	950 °C/NH_3/15 h	3.971(2)	pale brown
$La_{0.25}Ba_{0.75}Ti$	900 °C/NH_3/15 h	–	khaki
$La_{0.25}Ba_{0.75}Ti$	950 °C/NH_3/15 h	3.982(1)	dark green
$La_{0.75}Sr_{0.25}Ti$	950 °C/NH_3/15 h	3.928(2)	red
$La_{0.50}Sr_{0.50}Ti$	950 °C/NH_3/15 h	3.9187(4)	orange
$La_{0.25}Sr_{0.75}Ti$	950 °C/NH_3/15 h	3.917(1)	ocher
$La_{0.10}Sr_{0.90}Ti$	850 °C/NH_3/15 h	–	green
$La_{0.10}Sr_{0.90}Ti$	950 °C/NH_3/15 h	3.9130(3)	apple green

[a] Refined values (using Dicvol04[36]).

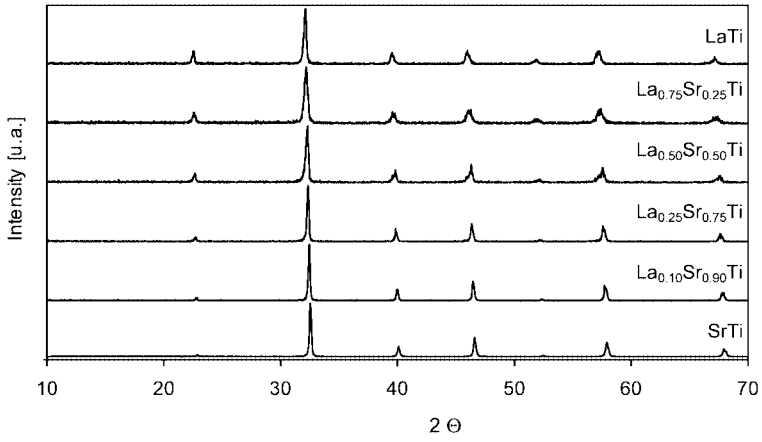

Figure 3. XRD patterns of the $La_{1-x}Sr_xTi(O,N)_3$ compositions (prepared at 950 °C) between the end terms of the solid solution.

either inductive effects or octahedral distortions. While changing the alkaline earth metal, similar color and also bandgap modifications have been observed in many phases, for example, in the perovskite-type oxynitrides, $CaTaO_2N$ (yellow), $SrTaO_2N$ (orange red), and $BaTaO_2N$ (red brown).[7,8,10,25–27] In this series, the atomic ratio O/N is constant and the modifications in the optical properties can only be explained by any changes in the structure and/or in the inductive effect relative to the choice of the alkaline earth metal. The characteristics of these phases are the following: $BaTaO_2N$ [cubic, bandgap = 1.8 eV; Ta–(O,N)–Ta = 180°], $SrTaO_2N$ [tetragonal, bandgap = 2.1 eV; Ta–(O,N)–Ta = 180° and 173.8°], $CaTaO_2N$ [orthorhombic, bandgap = 2.4 eV; Ta–(O,N)–Ta = 153.9°]. The linear evolution of the bandgap from $BaTaO_2N$ to $CaTaO_2N$ does not parallel a linear change in the Ta–(O/N)–Ta angles. As $BaTaO_2N$ and $SrTaO_2N$ display similar bond angles we expect similar bandgaps for both of them, which is not the

 © 2006 Wiley-VCH Verlag GmbH & Co. KGaA, Weinheim

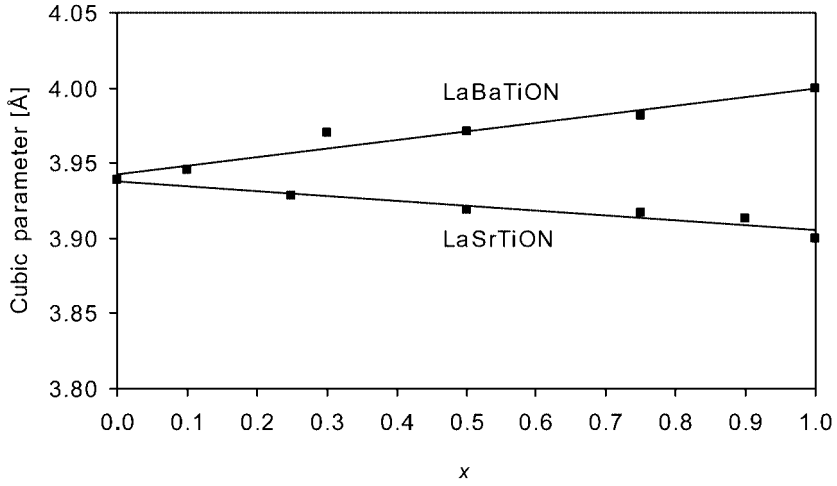

Figure 4. Variation of the unit-cell parameter in the $La_{1-x}Ba(Sr)_xTi(O,N)_3$ solid solutions.

case. Thus, the evolution of the bandgap value, and also the color, cannot only be the consequence of the deviation from linearity of the M–O–M bonds. The color change is due to several parameters including structure changes and the influence of the weaker inductive effect of strontium compared to that of barium, leading to a less covalent compound.

According to ref.,[24] the bandgap variation between $SrTiO_3$ (180°) and $CaTiO_3$ (156°) reaches 0.2 eV. However, the bond angles of $LaTiO_2N$ (160–167°) are closer to 180° than those of $CaTiO_3$, so we can expect a lower influence on the bandgap and a more diluted one for each of the intermediate compositions in the solid solution La–Sr–Ti–O–N. Between the two end members, $LaTiO_2N$ and $SrTiO_3$, the only visible effect in the bandgap position comes from the N/O substitution. The main consequence is an important red shift of the absorption edge. Thus, compared to the Ba-based system, for the same value of x, the absorption of the Sr-containing compositions is shifted towards lower wavelengths resulting in red and orange powders for x = 0.25 and x = 0.50, respectively, instead of the brown powders observed for the Ba-containing compositions. In the present system, the color of the powders varies progressively from the brown of $LaTiO_2N$ to the white of the oxide $SrTiO_3$ with the decrease in the nitrogen content. However, the x = 0.9 composition is also characterized by a bright green shade close to apple-green. This greenish color of the powder may be a consequence of the combination of a yellow hue and a black component. It is effectively known that a black-unsaturated yellow appears green, then khaki, and finally black.

We ascribe the black shade to the presence of a mixed-valent-state for titanium (Ti^{III}/Ti^{IV}). The origin of this phenomenon may be clarified according to two hypotheses. First, the reduction of titanium may occur directly in the oxynitride product. It is then necessary to take account of a decrease in the formal cationic charge and consequently of a smaller nitrogen content in the structure, as illustrated by the following formulations with x = 0.9:

$(La_{1-x}Sr_x)Ti^{IV}O_{2+x}N_{1-x} \rightarrow (La_{1-x}Sr_x)(Ti^{IV}_{1-y}Ti^{III}_y)O_{2+(x+y)}N_{1-(x+y)}$

$(La_{0.1}Sr_{0.9})Ti^{IV}O_{2.9}N_{0.1} \rightarrow (La_{0.1}Sr_{0.9})(Ti^{IV}_{1-y}Ti^{III}_y)O_{2.9+y}N_{0.1-y}$

Secondly, some reduced titanium may be present in a secondary black phase, TiO_xN_y. The powder then contains a mixture of a nitrogen-rich titanium oxynitride phase and a yellow $La_{0.1}Sr_{0.9}Ti(O,N)_3$ oxynitride. However, no secondary phase was detected by XRD analyses (Figure 3). From experience, it is well known that a very small amount of impurity, even indiscernible by XRD, may be sufficient to alter completely the color of the product and to overestimate nitrogen titration results. In order to avoid any reduction of titanium, ammonolysis experiments were carried out at lower temperatures (until 850 °C), but this did not allow for the stabilization of the higher oxidation state of titanium since a green shade was still observed. Grins et al. have reported similar color changes within the oxynitride solid solutions $AZr_xTa_{1-x}O_{2+x}N_{1-x}$ (A = Ca–Ba) without describing the hue progression.[16]

Nitrogen determination of the samples leads to the formulations listed in Table 2. Experimental contents are slightly higher than the calculated values (≈2%). In the case of the most greenish composition (A = Ba and x = 0.75), the observed deviation (≈4%) is more important and seems to validate the hypothesis of a nitrogen-rich secondary phase. In the strontium-based oxynitride series, the black component in the apple-green shade is not very marked and suggests an extremely low amount of titanium oxynitride TiO_xN_y, which does not considerably affect the measured nitrogen amount.

The optical characterization of $La_{1-x}Sr_xTi(O,N)_3$ oxynitrides by diffuse reflectance highlights several significant points (Figure 5). The plot of the corresponding spectra between the two end members of the solid solution confirms the shift of the absorption edge towards higher wavelengths with increasing nitrogen content. However, this shift is not progressive. Between the oxide $SrTiO_3$ and the oxynitride $La_{0.1}Sr_{0.9}Ti(O,N)_3$ the absorption edge moves from 375 to 500 nm – a shift of 125 nm – whereas it stays between 525 and 590 nm for the lanthanum-rich compositions. In an at-

 © 2006 Wiley-VCH Verlag GmbH & Co. KGaA, Weinheim

Table 2. Nitrogen contents and corresponding oxynitride formulations.

Cationic composition	N wt.-%$_{calcd.}$	N wt.-%$_{exp.}$	Experimental formulation
LaTi	6.02	6.1_7	$LaTiO_{1.96}N_{1.02}$
$La_{0.90}Ba_{0.10}Ti$	5.41	5.5_5	$La_{0.90}Ba_{0.10}TiO_{2.07}N_{0.92}$
$La_{0.70}Ba_{0.30}Ti$	4.21	4.4_3	$La_{0.70}Ba_{0.30}TiO_{2.27}N_{0.73}$
$La_{0.50}Ba_{0.50}Ti$	3.01	3.1_4	$La_{0.50}Ba_{0.50}TiO_{2.48}N_{0.52}$
$La_{0.25}Ba_{0.75}Ti$	1.50	2.0_5	$La_{0.25}Ba_{0.75}TiO_{2.62}N_{0.34}$
$La_{0.75}Sr_{0.25}Ti$	4.77	4.9_1	$La_{0.75}Sr_{0.25}TiO_{2.22}N_{0.77}$
$La_{0.50}Sr_{0.50}Ti$	3.36	3.5_2	$La_{0.50}Sr_{0.50}TiO_{2.47}N_{0.52}$
$La_{0.25}Sr_{0.75}Ti$	1.79	2.0_6	$La_{0.25}Sr_{0.75}TiO_{2.69}N_{0.29}$
$La_{0.10}Sr_{0.90}Ti$	0.74	0.9_1	$La_{0.10}Sr_{0.90}TiO_{2.88}N_{0.12}$

tempt to explain this nonlinearity, and despite the difficulty in calculating the band structure due to nitrogen/oxygen disorder, it is realistic to involve the following effects. Basically, the element located in the 12-fold coordination site does not directly influence the bandgap between the 2p(O) and 3d(Ti) bands, but rather it engenders an inductive effect on the Ti-(O,N) bond. Besides the effect of the large cation, nitrogen/oxygen substitutions modify the position of the valence band in a precise manner, so that the position of the absorption edge moves towards higher wavelengths. As nitrogen is less electronegative than oxygen, the energy level difference between the oxygen and nitrogen 2p orbitals [E_{2p}(O) = –14.8 eV, E_{2p}(N) = –13.4 eV (top of the valence band[28])] can simply explain the decrease in the bandgap between the valence and conduction bands. Also, as discussed above, by substituting La for Sr the decrease in the bond angles from 180° causes a small increase in the bandgap value that can act as a minor counter effect to the red shift (coupled with inductive effect variation) to explain parts of the nonlinearity of the bandgap values along the solid solution. By comparison with the oxide $SrTiO_3$, the absorption edge profile appears less steep and the spectral selectivity lower (Table 3), which is mainly a consequence of a lower crystallization state. We have already observed that the crystallization state of the powder influences the steepness of the diffuse reflectance spectrum in oxide systems. Thus, the absorption edge becomes steeper with an increasing crystallization state. This is probably linked to the better homogeneity of the environments of titanium. The average octahedron is $TiO_{4+2x}N_{2-2x}$, but because of the O/N disorder we consent that a large variety of O/N environments, with slightly different absorption properties, should exist around the titanium atoms, leading to the spreading of the absorption edge. Moreover, the level of the reflection plateau dramatically decreases with increasing nitrogen content. We have already observed, and not yet explained, such a phenomenon in several systems.[29,30] In the case of the composition x = 0.9 the absorption edge – located at 500 nm – should correspond to a yellow color although the powder appears "apple green". This result provides further confirmation of the presence of a black component. Thus, the alteration of the expected color is effectively due to the existence of partially reduced titanium, which is no longer totally stabilized under the reducing ammonia synthesis conditions used.

A more reactive oxide precursor was synthesized by the amorphous citrate route in order to stabilize the +4 oxidation state of titanium in the $La_{0.1}Sr_{0.9}Ti(O,N)_3$ oxynitride phase. This chimie douce process allows very fine and chemically homogeneous powders to be obtained rapidly. These powders are potentially able to manifest an enhanced reactivity with ammonia at lower temperatures.[31,32] Experimental data are listed in Table 4 for both the x = 0.9 and 1.0 compositions. A bright yellow powder is obtained after ammonolysis of the x = 0.9 precursor at 950 °C. Reduction phenomena did not occur with longer reaction times. The corresponding diffuse reflectance spectra, shown in Figure 6, reveal an absorption domain at the same wavelengths as that for the absorption of the greenish product obtained from the molten salt precursor. Moreover, a slight gain is noticed in the maximum value of the diffuse reflectance, in possible relation with the disappearance of the black component discussed previously. In addition, the experimental nitrogen content of this phase reaches 0.81 wt.-%, in excellent agreement with the calculated content (0.74 wt.-%), and corresponds to the following formulation $La_{0.10}Sr_{0.90}TiO_{2.89}N_{0.11}$. All these results confirm the hypothesis of the presence of a small amount of titanium oxynitride as an impurity in the former results, since the use of a more chemically homogeneous precursor solves the problem. Nevertheless, the green shade appears again for the composition x = 0.05, and the powder becomes yellowish green. In this case, a very small amount of dopant is present and hence it is difficult to come to a conclusion on the origin of the reduced titanium giving the green shade and also on the nature of the "impurity" phase. Many possibilities are of interest, such as the presence of a TiO_xN_y or $SrTi(O,N,\square)_3$ secondary phase. When the reaction is carried out under ammonia at 750 °C a pale green powder, without any marked yellow hue, is produced. It seems that under usual ammonolysis conditions the reduction of titanium occurs before the maximum nitrogen content is obtained.

To conclude, we have synthesized new oxynitride solid solutions for the systems $La_{1-x}A_xTiO_{2+x}N_{1-x}$ (A = Sr, Ba), where it is possible to tune progressively the color of the powders from brown ($LaTiO_2N$), to red, orange, yellow, and finally white ($SrTiO_3$) with the variation of both nitrogen and lanthanum contents. The green shade observed in the presence of low nitrogen contents is attributed to mixed-

 © 2006 Wiley-VCH Verlag GmbH & Co. KGaA, Weinheim

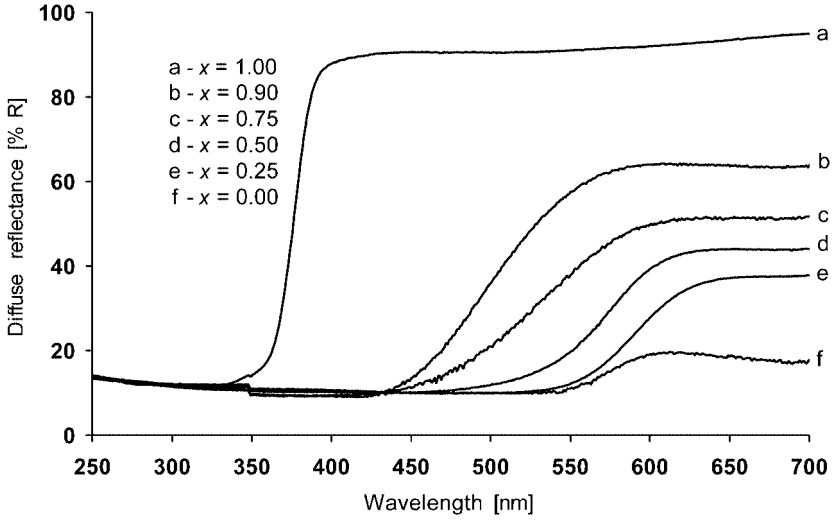

Figure 5. Diffuse reflectance spectra of $La_{1-x}Sr_xTi(O,N)_3$ compositions.

Table 3. Diffuse reflectance data of the oxynitride $La_{1-x}Sr_xTi(O,N)_3$ series obtained from precursors prepared by molten salt synthesis.

Composition	$\lambda \pm \Delta\lambda$ [nm]	*E*g [eV]
$SrTiO_3$	376 ± 14	3.31
$La_{0.10}Sr_{0.90}Ti(O,N)_3$	497 ± 63	2.49
$La_{0.25}Sr_{0.75}Ti(O,N)_3$	533 ± 60	2.27
$La_{0.50}Sr_{0.50}Ti(O,N)_3$	574 ± 38	2.07
$La_{0.75}Sr_{0.25}Ti(O,N)_3$	590 ± 33	2.02
$LaTiO_2N$	574 ± 30	1.96

valent titanium present in a black nitrogen-rich phase, TiO_xN_y. An attenuation of this reduction phenomenon is detected when using more chemically homogeneous and reactive precursors prepared by the amorphous citrate route. Such processes create suitable solutions to optimize the properties of (oxy)nitride materials for optical applications (colored pigments, visible-light photocatalysts). Avoiding such parasitic colors is a major synthetic problem in the preparation of light-colored materials for promising appli-

Table 4. Experimental data of the synthesis of $La_{0.1}Sr_{0.9}Ti(O,N)_3$ oxynitrides using the citrate route.

Cationic composition	Experimental parameters	Color	$\lambda \pm \Delta\lambda$ [nm]
SrTi	950 °C/air/15 h	white	376 ± 20
$La_{0.10}Sr_{0.90}Ti$	950 °C/NH_3/15 h	bright yellow	–
$La_{0.10}Sr_{0.90}Ti$	950 °C/NH_3/2 × 15 h	bright yellow	496 ± 57
$La_{0.05}Sr_{0.95}Ti$	750 °C/NH_3/15 h	pale green	–
$La_{0.05}Sr_{0.95}Ti$	900 °C/NH_3/2 × 15 h	pale yellow/green	483 ± 55
$La_{0.05}Sr_{0.95}Ti$	950 °C/NH_3/15 h	green	–

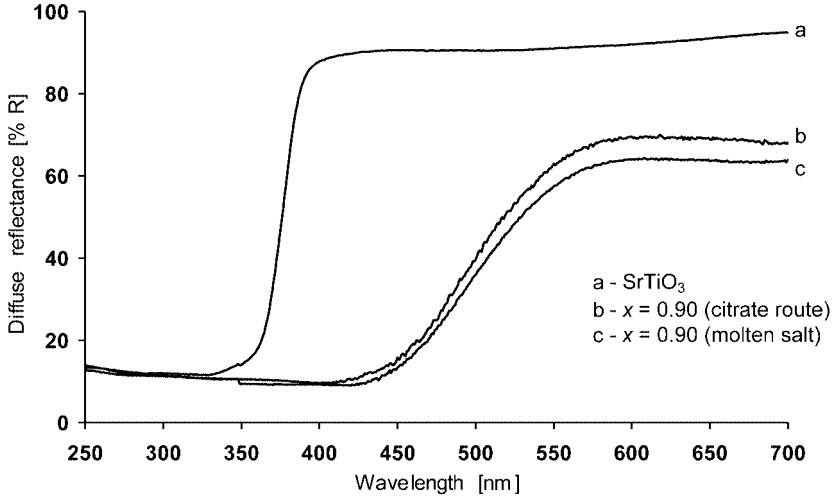

Figure 6. Comparison of the diffuse reflectance spectra of $La_{0.10}Sr_{0.90}TiO_{2.89}N_{0.11}$ prepared by ammonolysis of the molten salt and citrate precursors.

 © 2006 Wiley-VCH Verlag GmbH & Co. KGaA, Weinheim

cations such as novel UV absorbers. Nevertheless, the interest in oxynitride solid-solution domains relies on the ability to tune the absorption edge position towards 400 nm, which is the limit between the UV and the visible ranges.

Experimental Section

Synthesis of Oxide Precursors: Lanthanum-modified titanates were obtained using both a modified ceramic route and by taking advantage of the amorphous citrate route, a chimie douce method, which gives the oxide precursors an enhanced homogeneity and reactivity towards ammonia.

Solid-State Route: $La_{1-x}A_xTiO_{3.5-x/2}$ precursors (x = 0, 0.25, 0.5, 0.75, 0.9) were prepared by heating a stoichiometric mixture of La_2O_3 (99.99%, Alfa Aesar), $BaCO_3$ (99%, Acros), $SrCO_3$ (99%, Alfa Aesar), and TiO_2 (Degussa, P25) in a molten salt medium. The melt content, corresponding to the eutectic mixture 50 mol-% NaCl and 50 mol-% KCl, was determined to form 50 wt.-% of the total reactants weight.[33] The corresponding mixture was heated at 1000 °C for 15 h in a muffle furnace. The resulting products were washed using distilled water and absolute ethyl alcohol, and then dried at 150 °C.

Amorphous Citrate Route: Among numerous chimie douce type processes that have been developed to prepare oxide powders in order to improve their quality (purity, chemical homogeneity, etc.) and their reactivity the process involving citric acid as a complexing agent has been preferentially used. It is not, strictly speaking, a classic sol-gel process in the usual sense in that the gel is not formed by a metal–oxygen–metal network, but rather from calcination of metal–organic complexes, thus producing ultra fine reactive powders with an excellent chemical homogeneity.[34] In order to characterize any influence of the synthesis route, the x = 0.9 precursor for A = Sr was also prepared using this route. Lanthanum oxide (La_2O_3, 99.99%, Alfa Aesar), strontium carbonate ($SrCO_3$, 99%, Alfa Aesar), and titanium tetrabutoxide ($C_{16}H_{36}O_4Ti$, 99%, Acros) were used as starting materials and dissolved in a diluted nitric acid solution. Citric acid ($C_6H_8O_7$, Merck, > 99%) dissolved in a minimum amount of water was added to the solution in the proportion of one mole per cation valence, the addition being followed by a 30 min stirring step at 120 °C. Since the complexation of cations by citric acid is improved at pH ≥ 7, the acidic solution was neutralized by an ammonia solution (25%, Merck),[35] then stirred at 150 °C for 15 min to promote chelate formation. The liquid was progressively heated to 250 °C, leading after 15 h to an expanded black solid residue. This solid was finally ground and calcined at 600 °C in an alumina crucible until total elimination of carbon had occurred.

Thermal Ammonolysis: Nitridation reactions were carried out in alumina boats placed inside an electric furnace through which ammonia gas flowed at 40–50 $L\,h^{-1}$. The temperature was raised to 950–1000 °C with a heating rate of 10 °C min^{-1}. After a reaction time of 15 h the furnace was switched off and the nitrided powders were cooled to room temperature under a pure nitrogen atmosphere.

X-ray Diffraction: XRD powder patterns were recorded using a Philips PW3710 diffractometer operating with Cu-K_α radiation (λ = 1.5418 Å). X′PERT software – Data Collector, Graphics, and Identify – were used for recording, analysis, and phase matching of the patterns, respectively. The lattice parameters were refined using Dicvol04.[36]

Elemental Analysis: Nitrogen and oxygen contents were determined with a LECO TC-436 analyzer using the inert gas fusion method. Nitrogen was detected as N_2 by thermal conductivity and oxygen as CO_2 by infrared detection. The apparatus was calibrated using N_2 and CO_2 gas (purity ≥ 99.95%) as well as ε-TaN as a nitrogen standard.[37]

UV/Vis Spectrophotometry: Diffuse reflectance spectra were collected using a Varian Cary 100 Scan spectrometer equipped with the Varian WinUV software and the integrating sphere Labsphere (DRC-CA-30I). Prior to measurements, the absolute reflectance of the samples was calibrated with a certified "spectralon" standard (Labsphere Cie). Experimental data were collected within the 250–800 nm range with a 1 nm step and 0.5 s integration time. The position of the absorption edge was determined graphically at the inflection point of the curve and the value of the optical gap using the theory of Kubelka–Munk.[38]

[1] F. Cheviré, Thesis no. 3061, Université de Rennes 1, France, **2004**.
[2] D. Li, H. Haneda, S. Hishita, N. Ohashi, *Mater. Sci. Eng. B* **2005**, *117*, 67–75.
[3] D. Yamasita, T. Takata, M. Hara, J. N. Kondo, K. Domen, *Solid State Ionics* **2004**, *172*, 591–595.
[4] M. Hara, T. Takata, J. N. Kondo, K. Domen, *Catal. Today* **2004**, *90*, 313–317.
[5] A. Kasahara, K. Nukumizu, T. Takata, J. N. Kondo, M. Hara, H. Kobayashi, K. Domen, *J. Phys. Chem. B* **2003**, *107*, 791–797.
[6] R. Marchand, F. Pors, Y. Laurent, *Rev. Int. Tempér. Réfract. Fr.* **1986**, *23*, 11–15.
[7] F. Pors, R. Marchand, Y. Laurent, P. Bacher, G. Roult, *Mater. Res. Bull.* **1988**, *23*, 11–15.
[8] F. Pors, P. Bacher, R. Marchand, Y. Laurent, G. Roult, *Mater. Res. Bull.* **1988**, *23*, 1447–1450.
[9] F. Pors, P. Bacher, R. Marchand, Y. Laurent, G. Roult, *Rev. Int. Tempér. Réfract. Fr.* **1988**, *24*, 239–246.
[10] Y.-I. Kim, P. M. Woodward, K. Z. Baba-Kishi, C. W. Tai, *Chem. Mater.* **2004**, *16*, 1267–1276.
[11] R. Marchand, F. Pors, Y. Laurent, *Ann. Chim. Fr.* **1991**, *16*, 553–560.
[12] J. Etourneau, J. Portier, F. Ménil, *J. Alloys Compd.* **1992**, *188*, 1–7.
[13] H.-C. Zur Loye, J. D. Houmes, D. S. Bem, *The Chemistry of Transition Metal Carbides and Nitrides* (Ed.: Ted Oyama), Blackie Academic & Professional, **1996**, *8*, 155.
[14] S. J. Clarke, B. P. Guinot, C. W. Michie, M. J. C. Calmont, M. J. Rosseinsky, *Chem. Mater.* **2002**, *14*, 288–294.
[15] M. Jansen, H. P. Letschert, *Nature* **2000**, *404*, 980–982.
[16] M. Jansen, H. P. Letschert, *European Patent no. 0627373,* **1995**.
[17] J. Grins, G. Svensson, *Mater. Res. Bull.* **1994**, *29*, 801–809.
[18] N. Diot, *Thesis no. 2222*, Université de Rennes 1, France, **1999**.
[19] F. Pors, R. Marchand, Y. Laurent, *J. Solid State Chem.* **1993**, *107*, 39–42.
[20] P. Maillard, F. Tessier, E. Orhan, F. Cheviré, R. Marchand, *Chem. Mater.* **2005**, *17*, 152–156.
[21] E. Günther, M. Jansen, *Mater. Res. Bull.* **2001**, *36*, 1399–1405.
[22] G. Hitoki, T. Takata, J. N. Kondo, M. Hara, H. Kobayashi, K. Domen, *Electrochem.* **2002**, *70*, 463–465.
[23] R. D. Shannon, *Acta Crystallogr. Sect. A* **1976**, *A32*, 751–767.
[24] H. W. Eng, P. W. Barnes, B. M. Auer, P. M. Woodward, *J. Solid State Chem.* **2003**, *175*, 94–109.
[25] F. Pors, P. Bacher, R. Marchand, Y. Laurent, G. Roult, *Rev. Int. Hautes Tempér. Réfract.* **1987**, *24*, 239–246.
[26] E. Günther, R. Hagenmayer, M. Jansen, *Z. Anorg. Allg. Chem.* **2000**, *626*, 1519–1525.
[27] S. J. Clarke, K. A. Hardstone, C. W. Michie, M. J. Rosseinsky, *Chem. Mater.* **2002**, *14*, 2664–2669.
[28] R. Hoffmann, *J. Chem. Phys.* **1963**, *39*, 1397–1412.

 © 2006 Wiley-VCH Verlag GmbH & Co. KGaA, Weinheim

[29] F. Cheviré, F. Tessier, R. Marchand, *Sil. Ind.* **2004**, *69*, 159–163.
[30] N. Diot, O. Larcher, R. Marchand, J. Y. Kempf, P. Macaudière, *J. Alloys Compd.* **2001**, *323–324*, 45–48.
[31] F. Cheviré, F. Tessier, R. Marchand, *Mater. Res. Bull.* **2004**, *39*, 1091–1101.
[32] P. Maillard, F. Tessier, E. Orhan, F. Cheviré, R. Marchand, *Chem. Mater.* **2005**, *17*, 152–156.
[33] P. A. Fuierer, R. E. Newnham, *J. Am. Ceram. Soc.* **1991**, *74*, 2876–2881.
[34] F. Tessier, R. Marchand, *J. Solid State Chem.* **2003**, *171*, 143–151.
[35] A. Douy, P. Odier, *Mater. Res. Bull.* **1989**, *24*, 1119–1126.
[36] A. Boultif, D. Louer, *J. Appl. Crystallogr.* **2004**, *37*, 724–731.
[37] M. Dopita, B. Wollein, D. Rafaja, W. Gruner, W. Lengauer, *Defect and Diffusion Forum, Diffusion in Materials*, DIMAT-2000, **2001**, *194–199*, 1607–1612.
[38] D. Kubelka, L. Munk, *Z. Techn. Physik* **1931**, *12*, 593–601.

Received: August 23, 2005
Published Online: February 2, 2006

 © 2006 Wiley-VCH Verlag GmbH & Co. KGaA, Weinheim